An Experimental Study of Thrust Dependence on Magnetic Field in an Electrodeless Inductive Plasma Accelerator

IEPC 2019-537

Presented at the 36th International Electric Propulsion Conference
University of Vienna • Vienna, Austria
September 15-20, 2019

Akira Tatsuno[1], Kazuya Yaginuma[2], Hokuto Sekine[1], Hiroyuki Koizumi[1, 2] and Kimiya Komurasaki[2]

[1]*Department of Advanced Energy, University of Tokyo, 5-1-5, Kashiwanoha, Kashiwa, Chiba 277-8561, Japan*
[2]*Department of Aeronautics and Astronautics, University of Tokyo, 7-3-1, Hongo, Bunkyo-ku, Tokyo 113-8656, Japan*

Abstract: Electric propulsion which has low thrust power ratio cannot be used in the manned mission because the exposed time by cosmic rays must be short. The concept of RIPAL is completely electrodeless and get thrust by electromagnetic acceleration. In this work, we obtained distributions of the electron density and the thrust by using a double probe and a horizontal pendulum type thrust measurement. From these data, we clarified the relationship between the static magnetic field and the thrust.

Nomenclature

A	=	area of target, m^2
B	=	magnetic flux density, T
d	=	diameter of a xenon ion, m
E	=	electric field, V/m
e	=	elementary charge, C
F	=	force, N
j	=	current density, A/m^2
K_{iz}	=	rate constant, m^{3}s^{-1}
k	=	Boltzmann constant
M	=	mass of a xenon ion, kg
m	=	mass of an electron, kg
n_e	=	electron density, m^{-3}
n_i	=	ion density, m^{-3}
n_n	=	neural particle density, m^{-3}
p	=	pressure, Pa
R_p	=	total resistance, Ω
T_e	=	electron temperature, K
r	=	radial distance, m
V	=	electron velosity, m/s
z	=	axial distance, m
ΔR_p	=	resistance of microscopic ring, Ω
Δs	=	area of microscopic rectangle, m^2
η	=	resistivity, Ωm
ν	=	collision frequency of electron, s^{-1}
Ω_{H}	=	hall parameter

I.Introduction

HIGH power electrodeless thrusters are developped all over the world. In electrode thrusters, electrode erosion rarely limits lifetime and the quasi-neutral plasma is exhausted, eliminating the need for a cathode. There is

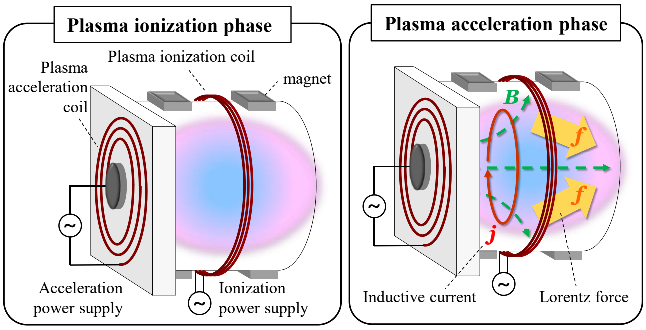

Figure 1. The concept of RIPAL.

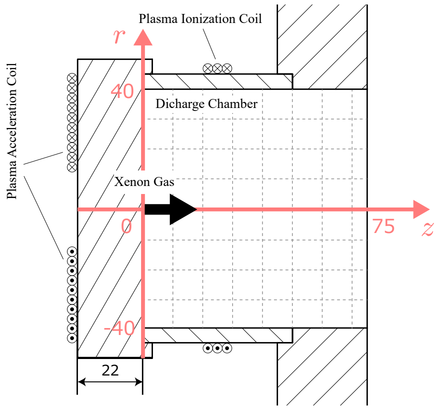

Figure 2. The sectional view of discharge chamber. The length and diameter of the discharge chamber is 75 mm and 80 mm.

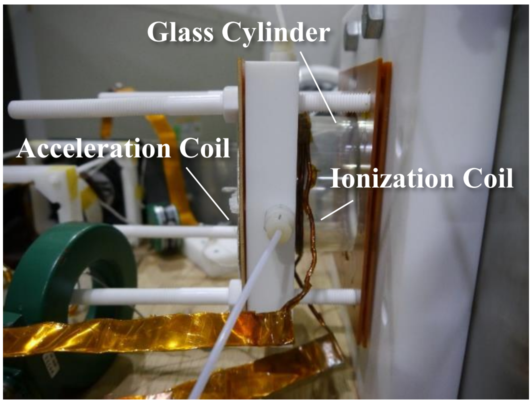

Figure 3. A picture of dischaege chamber.

in some research and development of electrodeless propulsion. For example, VASIMR [1] uses electrothermal acceleration and PIT [2] and FARAD [3] use induction acceleration. Magnetic nozzle thrusters [4] and HEAT [5] are propulsion systems that use helicon plasma. However, none have achieved high propulsion efficiency in steady operation.

Among them, RIPAL (Radio-frequency Inductive Plasma Accelerator with Low-aspect Ratio Plasma) was proposed by Yaginuma et al. [6) - 8)], which is an electrodeless propulsion system using inductive acceleration of RF plasma. Figure 1 shows the principle of thrust generation of RIPAL and Figure 2 and Figure 3 show a sectional view and picture of discharge chamber. There are two stages of thrust generation of this propulsion unit, which consists of the ionization phase and the acceleration phase. In the plasma ionization phase, 13.56 MHz is applied to the plasma ionization coil wound around a glass cylinder. The propellant in it flowing from the upstream side is ionized by RF to generate plasma. In the plasma acceleration phase, while plasma is being generated, several hundred kHz is applied to the plasma acceleration coil attached to the bottom surface of a glass cylinder. An induced current j is induced in the plasma and the Lorentz force $F = j \times B$ is generated by the interaction with induction magnetic field B produced by the coil to accelerate the plasma. In previous research, an induced current density j is measured by a magnetic probe [8]. The current rotates in azimuthal direction and its quantity is about 2 - 4 kA.

Induction acceleration is a condition close to collisionless plasma, so it can solve the frozen flow loss that is a problem of electrothermal acceleration. In addition, RIPAL uses a variable magnetic field, which can solve the problem of separation from the magnetic nozzle and HEAT problem. PIT and FARAD are the driving forces similar to RIPAL. Using the interaction between the variable magnetic field and the induced current is the same, but with PIT, the capacitor increases when the power is increased, and with FARAD, the plasma generator and plasma accelerator are separated, resulting in increased plasma loss. RIPAL generates plasma at radio frequency, so no capacitor is required. In addition, since the generation part and acceleration part are the same, plasma loss is reduced. Considering these facts, RIPAL is a powerful propulsion system that solves the problems encountered in previous studies and achieves high power thrust.

Yaginuma experimentally demonstrated thrust generation by the proposed principle using a 1 kW class test [6]. However, high thrust and propulsion efficiency have not yet been achieved [6) - 8)]. The main problem of RIPAL is its low thrust. In order to increase that, it is necessary to increase the low electron density which is currently about 8.0×10^{17} m^{-3}. Strengthen the static magnetic field in a discharge chamber is the most effective way to achieve the high electron density. However, the relationship between the thrust and the static magnetic field has not been clarified in this system.

Therefore, in this study, the static magnetic field is changed by using ferrite and neodymium magnets placed on the side or bottom of the propulsion system, and experimentally clarify the relationship between the thrust and the static magnetic field.

II. Analytical model

In order to increase the thrust, it is necessary to increase the azimuthal current. If the electron density is increased by increasing the static magnetic field, the azimuthal current is expected to increase. On the other hand, the axial static magnetic field becomes resistant to the azimuthal current. In order to evaluate these effects together, the equation of the azimuthal current is calculated from the equation of motion and the generalized Ohm's law.

By using a current density $\boldsymbol{j}$, a magnetic field $\boldsymbol{B}$ and a pressure p , the equation of motion in bulk plasma is

$$Mn_i\frac{D\boldsymbol{V}}{Dt} = \boldsymbol{j}\times\boldsymbol{B} - \boldsymbol{\nabla}p, \tag{1}$$

where M is the mass of a xenon ion and n_i is the ion density. $\boldsymbol{j}\times\boldsymbol{B}$ is the Lorentz force and $\boldsymbol{\nabla}p$ is the slope of pressure. This equation shows that the total thrust includes those due to pressure and those due to Lorentz force, and the Lorentz force is proportional to the magnitude of the current density. The current density can be discribed from the Ohm's law as

$$en_e\eta\boldsymbol{j} + \boldsymbol{j}\times\boldsymbol{B} = en_e(\boldsymbol{E}+\boldsymbol{V}\times\boldsymbol{B}) + \boldsymbol{\nabla}p, \tag{2}$$

where e is the elementary charge, n_e is the electron density, η is the resistivity, E is the electric field and $\boldsymbol{V}$ is the electron velosity. Assuming that $B_\theta = 0$ and $\boldsymbol{E}$ is dominant over $\boldsymbol{V}\times\boldsymbol{B}$ and $\boldsymbol{\nabla}p$, we have

$$j_\theta = \frac{1}{\eta(1+\Omega_{\mathrm{H}}^2)}E_\theta. \tag{3}$$

In order to increase the azimuthal current density, it is necessary to reduce the resistivity η_θ which is

$$\eta_\theta = \eta(1+\Omega_{\mathrm{H}}^2) = \frac{m\nu}{e^2 n_e}(1+\Omega_{\mathrm{H}}^2), \tag{4}$$

where m is the mass of the electron, ν is the collision frequency of the electron and Ω_{H} is the hall parameter of the static magnetic field. The collision frequency and the hall parameter are written as

$$\nu = n_n K_{iz,en} + n_i K_{iz,ei} \tag{5}$$

$$\Omega_{\mathrm{H}} = \frac{eB}{m\nu}, \tag{6}$$

where n_n and n_i are density of neural particles and ions, and $K_{iz,en}$ and $K_{iz,ei}$ are the rate constant between an electron and neural paticles and between an electron and ions. $K_{iz,en}$ is calculated from momentum transfer cross sections for elastic electron scattering [9], and $K_{iz,ei}$ is written as

$$K_{iz,ei} = \frac{e^4}{16\pi\epsilon_0^2 m^2 v_{\mathrm{th}}^3}\ln\Lambda \tag{7}$$

d is a diameter of a xenon ion, v_{th} is the thermal velosity, ϵ_0 is the dielectric constant of vacuum and $\ln\Lambda$ is the coulomb logarithm.

The resistivity include both the static magnetic field and the electron density. The static magnetic field increases the resistivity but the electron density reduces it. By calculating the resistance in every experiment, the relationship between the static magnetic field and the thrust becomes clear.

Assuming that the resistivity in the azimuthal direction is constant and the distance from the center axis to a microscopic rectangle with area Δs is r , the resistance of the ring at z , r becomes

$$\Delta R_p = \eta_\theta\frac{2\pi r}{\Delta s}. \tag{8}$$

Assuming that all the resistances thus obtained are connected in parallel, the total resistance R_p is calculated as

$$\frac{1}{R_p} = \sum\frac{1}{\Delta R_p} \tag{9}$$

$$R_p = \frac{2\pi}{\Delta s}\left(\sum\frac{1}{r\eta_\theta}\right)^{-1}. \tag{10}$$

In this study, the relationship between the thrust and the total resistance is used to evaluate effects of the static magnetic field. The calculation range of R_p is 10 < $|r|$ < 25, 0 < z < 50 in Figure 2.

III.Experimental method

A. Vacuum system

The experiments in this study were conducted in a stainless steel vacuum chamber with Ø1.4 m and a length of 3.0

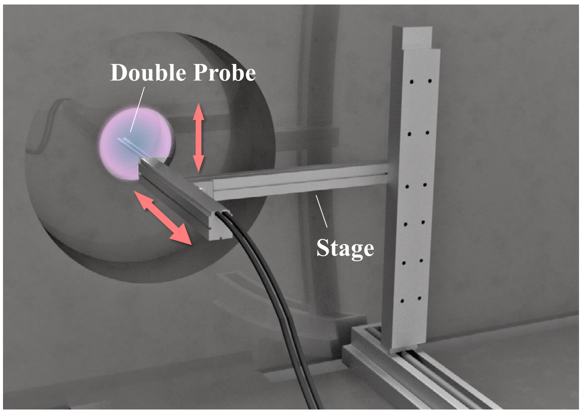

Figure 4. Two-demensional measuring equipment (CAD). The stage moves in vertical and horizontal direction.

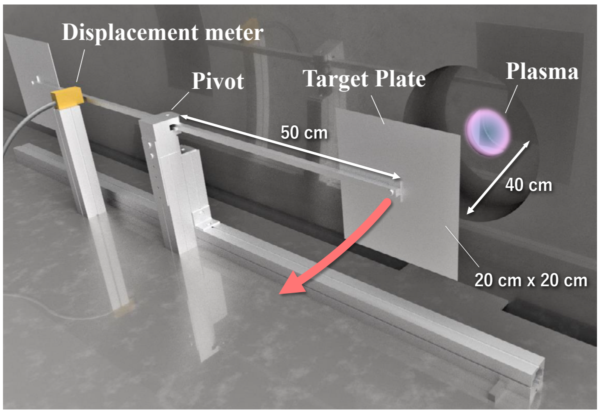

Figure 5. Thrust measurement equipment (CAD). The displacement of the target is measured with a laser displacement meter on the opposite side.

m. During the experiment, a cryopump with a pumping speed of 10000 L / s (N_2) was operated at all times, and the back pressure of the chamber during the experiment was 2.2 × 10^{-2} Pa.Ø

B. Discharge chamber

The discharge chamber consists of a plasma excitation coil, a high frequency power supply, and a matching circuit. In the case of a plasma excitation coil, a Ø2 enameled wire is wound three times around a Ø90 glass tube. The high frequency power supply applies a 13.56 MHz frequency and a maximum output power of 400 W to the plasma ionization coil through a matching circuit. In this experiment, 400 W was introduced. Figure 2 shows a cross-sectional view of the discharge chamber.

C. Acceleration circuit

The plasma acceleration circuit comprises a plasma acceleration coil, a high frequency power supply, and a matching circuit. The plasma acceleration coil is attached to the bottom surface of the glass tube as a 10-turn planar coil. A high frequency power supply applies a frequency of 100 - 999 kHz and a maximum output voltage of 2 kW to the plasma acceleration coil through a matching circuit. In this experiment, the frequency is 522 kHz and input power is 500 W.

D. Two-dimensional measuring equipment

The two-dimensional distribution measuring equipment is composed of a double probe, a motor driven biaxial stage, a bipolar power supply, and a function generator. The motor driven biaxial stage is shown in Figure 4. The probe curve was obtained by operating the bipolar power supply with the function generator. By attaching the double probe to the stage, it is possible to obtain a two-dimensional distribution of the electron temperature and electron density of the generated plasma. A double probe was prepared by placing a stainless-steel rod of Ø2 mm and length 500 mm in an insulating tube with an inner diameter of 3 mm, an outer diameter of 4 mm and a length of 400 mm and fixing with an aron ceramic. The tip is a surface probe, and it is a circle of Ø2 mm. Two probes are spaced 2 mm apart so that the sheaths of the electrodes are not covered. The biaxial stage can be operated from an external personal computer through a flange, and it operates according to the measurement program.

The double probe is swept to pass through all the lattices with z in the range of 0 to 80 and r in the range of -25 to 25, and at the same time the probe-to-probe voltage is swept from -150 V to 150 V with a function generator and a bipolar power supply. The electron density and the electron temperature were calculated using the double probe curve obtained at each point, and a distribution map was obtained by plotting it.

E. Thrust measurement

The thrust measurement is performed with a horizontal pendulum type thrust stand as shown in Figure 5. A 20 cm by 20 cm target is attached to one side of the arm of the horizontal pendulum and it is located 40 cm behind of the exit where plasma is exhausted. The length of the arm is 50 cm and magnets is attached to the other as a damper, and a torsion spring is attached to the center. The displacement of the target is measured with a laser displacement meter on the opposite side, and the thrust is calculated from the calibration factor which measured before and after experiment.

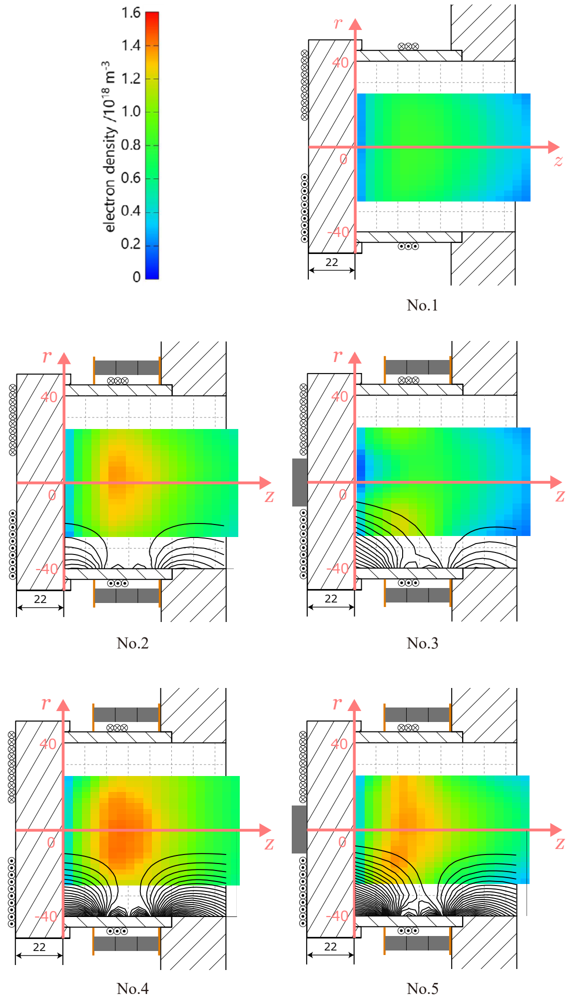

Figure 6. Results of the electron density measurement. These are measured with 400 W of the plasma generation power supply and 0 W of the plasma acceleration power supply.

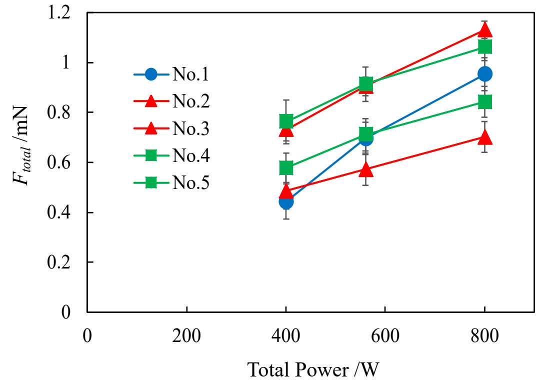

Figure 7. Result of thrust measurement.

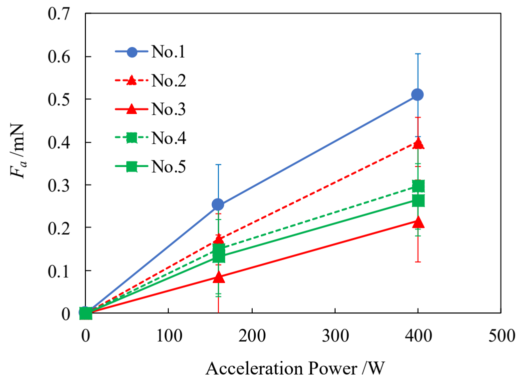

Figure 8. The acceleration power is plotted on the horizontal axis and the thrust increment is taken on the vertical axis.

IV.Experimental conditions

In this study, the mass flow rate (15 sccm), the input for ionization (400 W), and the input for acceleration (0 – 400 W) were the same, and the experiment was conducted using only the magnetic field shape in the discharge chamber as a parameter. Figure 6 shows the shape of the static magnetic field.

We use ferrite and neodymium magnets to change the shape and strength of the static magnetic field. In No.1 there is no magnet, in No.2 and 3 ferrite magnets are wound, and in No.4 and 5 neodymium magnets are wound on a discharge chamber. Only in No.3 and 5 there is a ferrite magnet in bottom surface. In Figure 6 the static magnetic field was solved under the axisymmetric assumption using the finite element method.

V.Result

The results of the electron density measurement were shown in Figure 6. They were measured with 400 W for ionization and 0 W for acceleration. No.1 which had no magnet was the lowest electron density. Focusing on No.2 and No.4, the electron density became large as the static magnetic field became stronger. The same applied to No.3 and No.5. In addition, in No.2 to No.5 the shape of the density distribution changed as the shape of the static magnetic field changed.

The results of the total thrust measurement was shown in Figure 7. The input for ionization was put by 400W and then the input for acceleration by 400W. The thrust of No.1 at 400W, only for ionization, was the smallest, but the rate of the thrust increase differed greatly with conditions.

The error of the thrust were the standard deviation of 3 times measurements and it was about 10%. The calibration factors for three times were 0.85 N/m, 0.84 N/m, and 0.77 N/m, and they were also within the range of about 10%. Therefore, the thrust error bar can be explained by the variation of the calibration factor.

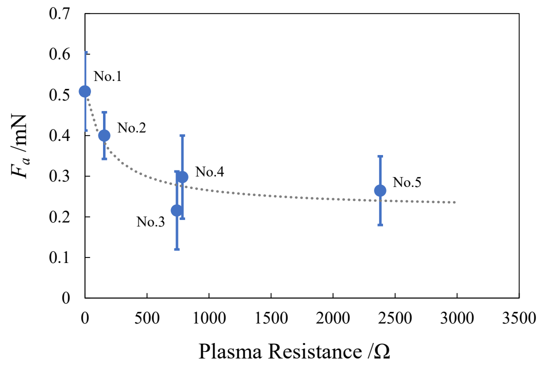

Figure 9. The relationship between the resistance value of each experiments and the thrust increment with 400 W acceleration power.

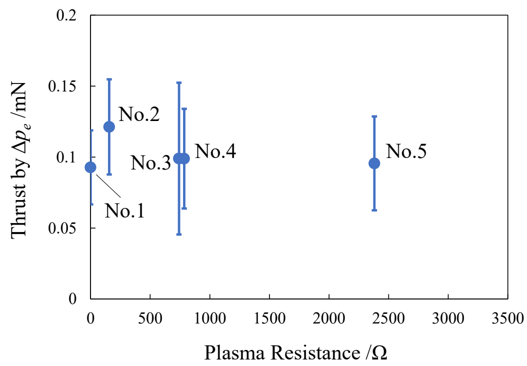

Figure 10. Thrust by downstream electron pressure at 400 W for acceleration under each experimental condition. Error bars represent the standard deviation of data measured 30 times.

The total thrust measured in Figure 7 can be separated as

$$F_{total} = F_i + F_a \tag{11}$$

F_i and F_a are the thrusts generated from ionization and acceleration, respectively. Figure 8 represented F_a , and although the electron density of No.1 was the lowest, F_a of it was the largest.

VI.Discussion

In Figure 9 the resistance was plotted on the horizontal axis and the thrust increment was taken on the vertical axis. The thrust increment decreased as the resistance increased. From the experiment number, as the static magnetic field was strengthened, the resistance became large, and as a result the thrust power ratio became small. In other words, enlarging the static magnetic field lead to increasing the electron density, but the resistance also increased and the thrust power ratio decreased.

The thrust measured by the thrust measurement equipment is written as

$$F = \dot{m}v + \Delta p_e A \tag{12}$$

where $\dot{m}$ is mass flow rate, v is velosity of plasma, p_e is electron pressure and A is area of the target.

Electron pressure $p_e = n_e k T_e$ in z = 480, where the thrust measurement equipment was put, was measured by using a double probe. The thrust by Δp_e was calculated with target area 20 × 20 mm and the result was shown in Figure 10. An error bar of each condition was overlapping, so it is difficult to find a significant difference in electron pressure. However, focusing on No.1 and No.5, there is a significant difference in F_a in Figure 9. From this, it can be seen that when plasma resistance increased, Fa decreased, but the thrust by Δp_e did not change.

Therefore, as the static magnetic field was strengthened, electron pressure did not change but velosity of plasma became smaller. It means that the induced current density $\boldsymbol{j}$ decreases.

VII.Conclusion

In order to increase the thrust of RIPAL, we changed the static magnetic field and clarify the dependence of thrust and static magnetic field. As the static magnetic field increases, the electron density increases, but the total plasma resistance taking them into account increases. The thrust increment decreases as the resistance increases. Therefore, enlarging the static magnetic field is inappropriate to increase the thrust in this system.

References

[1]Leonard, D., and Benjamin W., et al., "VASIMR Performance Results," *AIAA Joint Propulsion Conference and Exhibit*, 2010.

[2]Kurt, A., "Comprehensive Review of Planar Pulsed Inductive Plasma Thruster Research and Technology," *Journal of Propulsion and Power*, 2011, Vol. 27, No. 3, pp.513-531.

[3]Edgar, Y., and Kurt, A., "Faraday Acceleration with Radio-Frequency Assisted Discharge," *Journal of Propulsion and Power*, 2006, Vol. 22, No. 3, pp. 611-619.

[4]Takahashi, K., "Adiabatic Expansion of Electron Gas in a Magnetic Nozzle," *Physical review Letters*, 2018.

[5]Shinohara, S., "Research and Development of a Novel Electrodeless Plasma Rocket Engine Using a Helicon Source," *J. Plasma Fusion Res.* , 2015, Vol.91, No.6.

[6]Yaginuma, K., "Effects of Acceleration Coils on the Performance in an Electrodeless Inductive Plasma Accelerator," *60th Proceedings of*

the Space Sciences and Technology Conference, 2016.

[7]Matsuguma, T., "Modeling of the Induced Plasma Acceleration by the Eddy Current Analysis and Verification Experiment using 1 kW Class Thruster," Master's Thesis, University of Tokyo, 2017.

[8]Sekine, H. et al., "Azimuthal Induced Current Formation and Ion Acceleration in an Inductive Radiofrequency Plasma Thruster," IEPC-2019-A-775.

[9]Adibzadeh, M., & Theodosiou, C. E., "Elastic electron scattering from inert-gas atoms" *Atomic Data and Nuclear Data Tables*, 2005, Vol 91, Issue 1, pp 8 - 76.